Article

Constitutive Model of the Surface Roughening Behavior of Austenitic Stainless Steel

Abdul Aziz [1,*], Ming Yang [1], Tetsuhide Shimizu [1] and Tsuyoshi Furushima [2]

1   Graduate School of System Design, Tokyo Metropolitan University, 6-6-Asahigaoka, Hino, Tokyo 191-0055, Japan; yang@tmu.ac.jp (M.Y.); simizu-tetuhide@tmu.ac.jp (T.S.)
2   Department of Mechanical and Biofunctional Systems, Institute of Industrial Science, University of Tokyo, 4 Chome-6-1 Komaba, Meguro, Tokyo 153-8505, Japan; tsuyoful@iis.u-tokyo.ac.jp
*   Correspondence: abdul.azizayahnajib@gmail.com

Abstract: The martensitic phase transformation (MPT) is one of the most important factors that enhances the surface roughening of stainless-steel thin metal foils (TMF), such as SUS 304, compared to others without MPT, even in the same plastic strain. However, the conventional roughening model does not take into account the influence of MPT. In this study, the authors proposed a new constitutive model to express the surface roughening by taking the influence of MPT into account. The volume fractions of MPT for TMF of SUS304 in various grain sizes are accounted for quantitatively after the tensile test at room temperature and an elevated temperature, and the effect of MPT on the surface roughening is evaluated in comparison to using TMF of SUS316, in which MPT does not occur during plastic deformation. Then, a constitutive model of the surface roughening based on the experimental results is successfully built.

Keywords: surface roughening; martensitic phase transformation (MPT); work hardening (*n*)

1. Introduction

Micro-/meso-scaled parts have been widely used in electronics, automobiles, aerospace, and biomedicine in tandem with the ubiquitous trend of product miniaturization [1–6]. In this decade, the demand for micro parts has increased unabated. Stainless steels such as SUS 304 and SUS 316 have wide applications in the micro-manufacturing industry. The estimated rise in turnover from USD 15 to 35 billion in the last seven years [1–7] shows a growing demand for micro technical products, which is mainly driven by the rising trend of the miniaturization of products. The demand for miniaturization comes not only from customers, who desire more handy electronic devices and more integrated functions, but also from technical applications such as medical equipment, sensor technology, and optoelectronics [3,4,8]. All these products contain mechanical parts such as leverages, connector pins, resistor caps, screws, contact springs, and cheap lead frames [1–4,9,10].

To understand the mechanisms behind surface roughening in austenitic stainless steel, many studies have been conducted on stainless steel sheets [2,4,11–14]. It has been generally reported that surface roughening linearly increases with plastic strain [14–17] and is affected not only by plastic deformation conditions such as the strain ratio or strain path but also by material factors such as the grain size crystal structure, crystal orientation and texture [15,17–19]. When the austenitic stainless steel is subjected to plastic deformation, martensitic phase transformation (MPT) occurs [15,20–22]. MPT occurs as a result of the slip band intersection. The slip band intersection is the place of the martensitic embryo and then becomes MPT [23–35].

In early studies, surface roughening was examined experimentally. Yamaguchi et al. [17] showed that the degree of surface roughening in aluminum-killed steel sheets depended on the amount of equivalent plastic strain and the crystal grain size. Mahmudi et al. [18] concluded that surface roughening was caused by inhomogeneity of the material's

microstructure. The degree of development in surface roughening also depended on the strain rate and the crystal structure [5–15]. The rotation of the crystal orientation caused by plastic strain was the factor of surface roughening in steel and aluminum sheets. [6–15]. The deformation of interior crystal grains from the surface to the second layer could affect the surface unevenness in some kinds of metal [6–15]. The previous studies concluded that the surface roughening should be expressed as a function of plastic strain as $\Delta Ra = Ce_p$, where ΔRa is the increase in surface roughness, C is a constant, and e_p is the plastic strain level [25–34].

Furushima et al. [34] also concluded that surface roughening not only depends on the strain level but also depends on grain size. The surface roughening should be expressed as follows:

$$\Delta Ra = Ce_p \cdot Dg/t \tag{1}$$

where ΔRa is the increase in surface roughness, e_p is the plastic strain level, Dg is the grain size, and t is the thickness of the workpiece.

The authors have been working on SUS 304 and SUS 316 thin metal foils and found that surface roughening not only depends on the strain level and grain size but also depends on martensitic phase transformation (MPT) and grain misorientation (GMO). Thus, it is not enough if the surface roughening depends on the grain size and strain level. MPT is the one factor in SUS 304 thin metal foil (TMF) that enhances the surface roughening compared to SUS 316 TMF, in which the surface roughening in SUS 304 increases higher than SUS 316 TMF with the same grain size (Dg) and the same strain level at room temperature [20]. Furthermore, the influential factor of grain size does not explain the surface roughening behavior in thin metal foils since the influential factors such as MPT and GMO are also related to the grain size of the material. There is currently a lack of studies that create a theoretical model to express the effect of MPT and GMO on the surface roughening in austenitic stainless-steel foils. No theoretical model has determined the effect of MPT and GMO on the surface roughening behavior in various grain sizes. Thus, this study aims to build a theoretical model to express the effect of MPT and GMO on the surface roughening behavior with various grain sizes based on the experimental results of tensile tests using SUS 304 and SUS 316 thin metal foils (TMF).

2. Materials and Methods

2.1. Material

The result of the tensile test in our previous studies was utilized to analyze the volume fraction of MPT and GMO in this study. In this research, the author uses SUS 304 and SUS 316 thin metal foils of SUS 304 and SUS 316. The material condition for room [20] and elevated temperature [21] was similar to previous results, such as sample dimension, microstructure, grain size, and chemical composition. Room temperature was used to investigate the effect of MPT and GMO on the surface roughening behavior. High temperatures were used to investigate effect of resistance heating (RH) on the surface roughening behavior. Author uses two kinds of materials, SUS 304 and SUS 316. The thickness was 0.1 mm, the grain size (Dg) was 1.5 μm; SUS 304 and SUS 316 thin metal foils were 3.0 μm and 9.0 μm, respectively.

2.2. Method

The methodology of using room temperature [20] and elevated temperatures [21] has been explained in previous research. The methodology, in general, involves using uniaxial tensile stress state for five steps, and surface roughness is measured every step. After surface roughness is measured for five steps, phase transformation and grain misorientation are observed using SEM-EBSD method.

The surface roughening behavior was investigated at elevated temperatures using resistance heating method. The resistance heating was conducted at 500 °C for three minutes for every step of the tensile test. The emissivity of the sample was 0.94. The thermos sensor camera used in this experiment was Optris Xi-400, made in Japan. The

uniaxial tensile test used the AGX-50KNVD machine, with loading capacity of up to 50 KN. The uniaxial tensile test machine was produced by Shimadzu, Japan. The surface roughening behavior was investigated using OLS-5000 laser microscope produced by Olympus Co., Tokyo, Japan.

The volume fraction of MPT and GMO was calculated using the ImageJ technique, utilizing the volume fraction based on color. The technique for calculating $d\sigma/d\varepsilon$ slopes involved obtaining value of σ and value of ε.

3. Construction of the Constitutive Model

3.1. Influence of the Volume Fraction of MPT on Surface Roughening

The surface roughening increases with the strain level. Furthermore, the surface roughening in SUS 304 increases higher than in SUS 316 TMF coarse grain at room temperature [20]. The main reason for this is that the MPT spreads inhomogeneously in the case of coarse grains. Figure 1 shows that the MPT spreads homogeneously in fine grains, as shown in Figure 1a, and spreads inhomogeneously in coarse grains, as shown in Figure 1b [20].


Dg 1.5 µm as receive　　　　　　　　Dg 1.5 µm 25% strain

(a)

Dg 1.5 µm as receive　　　　　　　　Dg 1.5 µm 25% strain

(b)
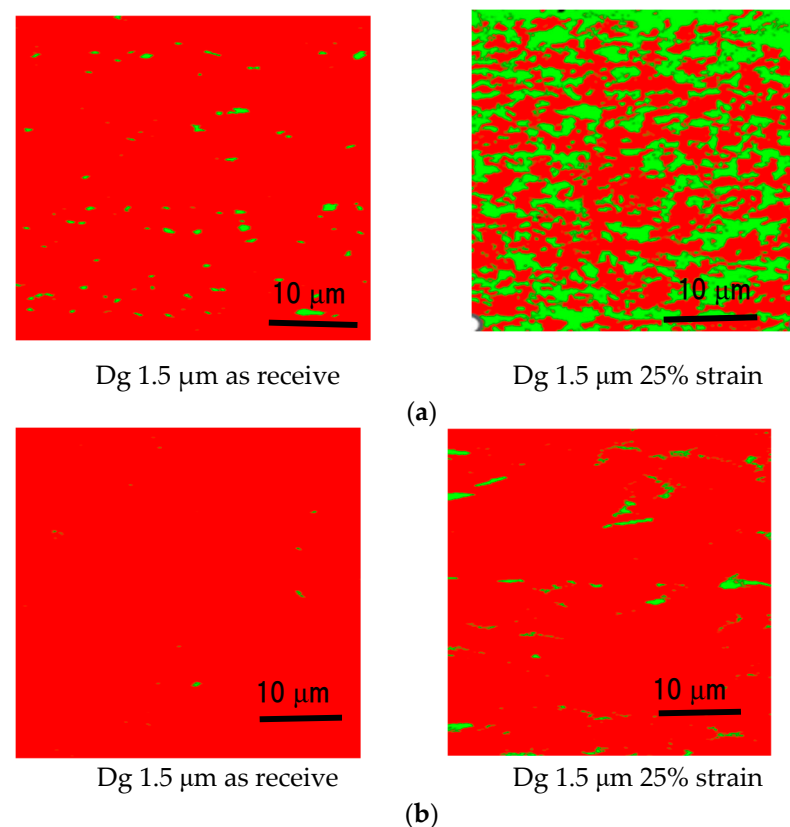
Figure 1. The phase map of SUS 304 fine grain and coarse grain [20]. (**a**) Fine grain; (**b**) Coarse grain.

The hardness structure with the martensitic phase is higher than that with grain misorientation at the same strain level, and the hardness of the material increases with the martensitic phase volume fraction [22]. The hardness increases hyperbolically with the FMPT. The increasing MPT affects the increasing FMPT and grain strength. The grain that contains MPT has a higher grain strength than the grain without MPT [22].

Figure 2 shows the volume fraction of martensitic phase transformation (F_{MPT}) at room temperature, and Figure 3 shows that at elevated temperatures. In Figure 2, the volume fraction of MPT (F_{MPT}) in SUS 304 TMF increases linearly with the strain level. The FMPT in the fine grains of SUS 304 increases higher than in coarse grains of SUS 304. MPT occurs due to the slip band intersection in the grains during the uniaxial tensile test. The

probability of the slip band intersection in the fine grains is higher than in the coarse grains; thus, the F_{MPT} in fine grains becomes much higher than in coarse grains.
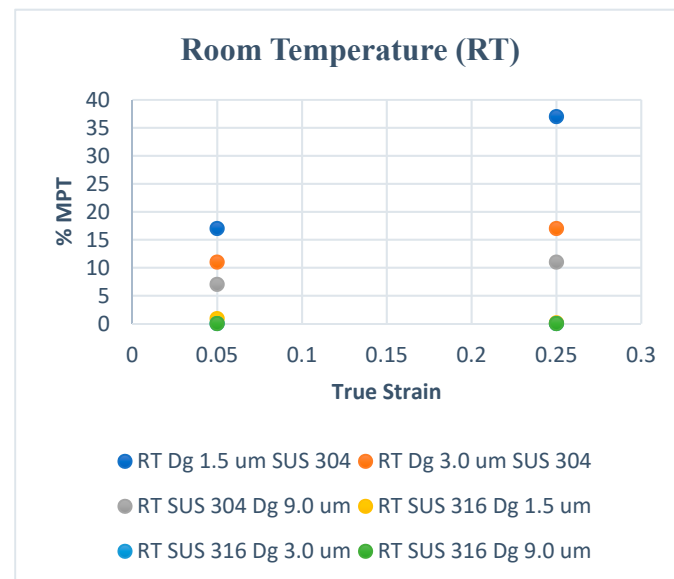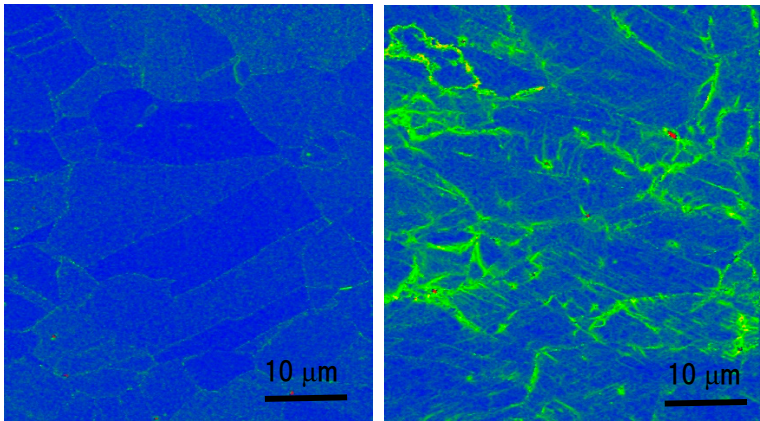

Figure 2. MPT at room temperature.
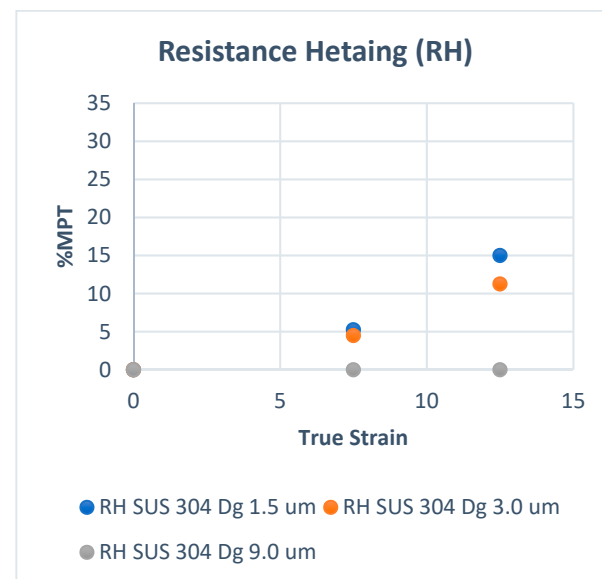
Figure 3. MPT at elevated temperatures.

Figure 3 shows that the F_{MPT} only increases linearly in the fine grains of SUS 304 TMF. The F_{MPT} was reduced significantly compared to room temperature. The F_{MPT} disappeared in coarse grains of SUS 304 TMF; because of the heating, the mobility of slip band movement increased, and the probability of slip band intersection decreased [21–27]. There is no F_{MPT} in SUS 316 TMF during the uniaxial tensile test, which uses resistance heating (RH).

Figures 4 and 5 show the KAM map in SUS 316 and SUS 304 coarse grains at room temperature [20]. In the KAM map, there are changes in FGMO until the 25.0% strain level.

Figures 6 and 7 show the GMO fraction (FGMO) in room temperature and elevated temperature. the FGMO increase proportional both in room and at elevated temperature. The FGMO decrease with increasing temperature both in fine and coarse grain. the FGMO in fine grains are higher than coarse grain both in room temperature (Figure 6) and at elevated temperature (Figure 7).

Dg 9.0 μm SUS 316 as received Dg 9.0 μm SUS 316 at 25.0 strain

Figure 4. KAM map of SUS 316 TMF.
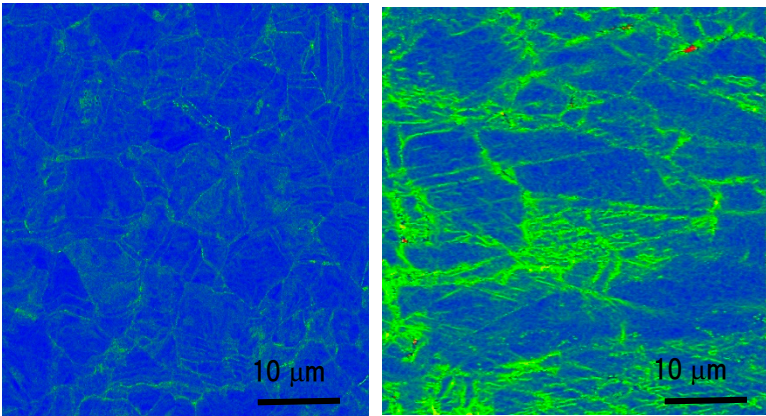
Dg 9.0 μm SUS 316 as received Dg 9.0 μm SUS 316 at 25.0 strain

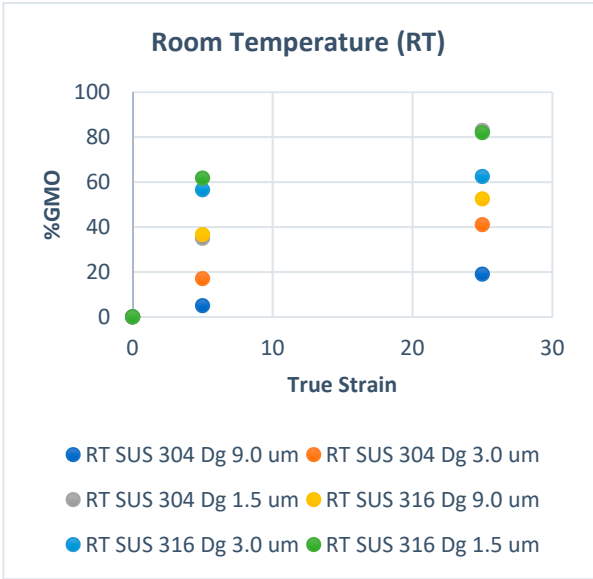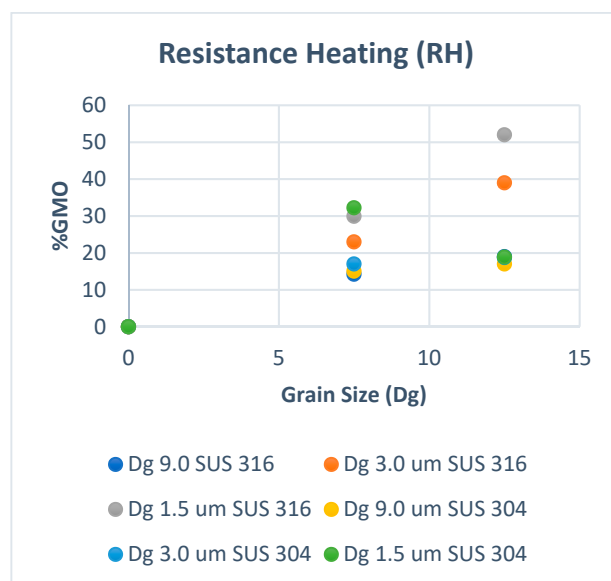**Figure 5.** KAM map of SUS 304 TMF.

Figure 6. The FGMO at room temperature.

Figure 7. The FGMO with resistance heating (RH).

The grain misorientation (GMO) is obtained from the calculation of the grain misorientation in the center of the grains and then averaged, which can be obtained from the KAM map of the SEM-EBSD analysis of the structures after deformation [20]. In this study, the volume fraction of GMO means the amount of GMO in a certain area. Figures 4 and 5 show a typical KAM map for SUS304 and SU316 TMFs in coarse grains from the KAM map of SEM-EBSD analysis in a previous study [20].

The FGMO counted for SUS 304 and SUS 316 TMF at room temperature and RH conditions shown in Figures 4 and 5. The F_{GMO} decreases with the grain size (Dg) and increases higher in SUS 316 compared to the SUS 304 TMF both in fine and coarse grains [20]. The GMO spread more inhomogeneously for the coarse grains of SUS 316 than the SUS 304 TMF. However, the surface roughness in SUS 304 coarse grains was higher than in SUS 316 TMF coarse grains since MPT only occurred at the same strain level in SUS 304 TMF. The higher surface roughness in SUS 304 could be affected by the MPT that spreads inhomogeneously in the grains at room temperature.

The quantity of GMOs decreases because of resistance heating both in SUS 304 and SUS 316 TMF, as shown in Figure 5. The F_{GMO} in the coarse grains of SUS 304 TMF decreases at high temperatures compared to room temperature. The F_{GMO} in SUS 316 TMF was higher than in SUS 304 TMF, and the inhomogeneous grain strength in SUS 316 TMF was higher than in SUS 304 at elevated temperatures. As a result, the surface roughness in SUS 316 TMF was higher than in SUS 304 TMF [21].

Dislocation density, F_{MPT}, and F_{GMO} increase proportionally with the strain level [24–29]. For fine grains, the FMPT and dislocation density in a grain become much higher than for coarse grains because the slip band intersection probability becomes much higher in fine grains than in coarse grains [24,27].

On the other hand, the work hardening index *n* is a macroscale view that may relate to surface roughening behavior. It is well known that when the *n* value of a material is higher than other material, the strain distribution is more uniform in the material than in the other one. Figures 8 and 9 show the work hardening index *n* for SUS 304 and SUS 316 TMF. The *n* value in SUS 304 at room temperature was lower than in SUS 316 TMF, but the hardness of SUS 304 TMF was higher than SUS 316 TMF at room temperature after the tensile test because the MPT occurred in SUS 304 TMF. In the elevated temperature (E.T.) condition, the *n* value of SUS 304 TMF was a little bit higher than SUS 316 TMF. It was found that there was no MPT in SUS 304 TMF, and the hardness of SUS 304 TMF and SUS 316 TMF became similar [21,22]. The work hardening for SUS 316 was higher than SUS 304 for every grain size (Dg) at room temperature. This means that SUS 316 TMF has a more uniform

deformation distribution in the workpiece. When a uniform deformation distribution in the workpiece occurs, the deformation in the grain becomes more homogeneous. The homogeneous grain deformation lowers the increase in surface roughness compared to inhomogeneous grain deformation at the same strain level. As a result, at room temperature, SUS 304 TMF shows higher surface roughness than SUS 316 TMF with the same strain level. On the other hand, at elevated temperatures, the work hardening of SUS 304 was higher than SUS 316 TMF. This means the SUS 304 TMF grain deformation distribution in the workpiece becomes more uniform or more homogeneous [21]. The increase in surface roughness in SUS 316 may become higher than in SUS 304 TMF with the same strain level. The phenomena of work hardening at room and high temperatures were different according to the occurrence or not of MPT.
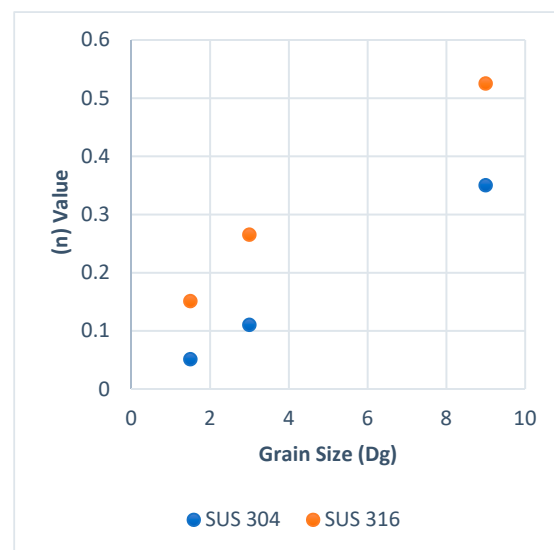
Figure 8. Work hardening room temperature.
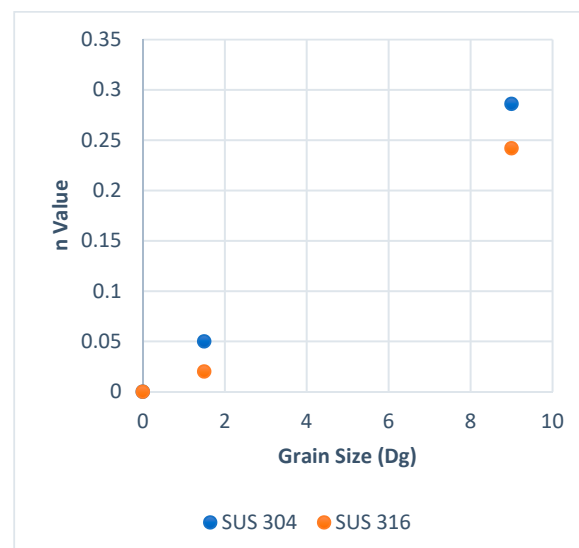
Figure 9. High work hardening at elevated temperature.

3.2. Quantitative Model

Based on the discussion in the previous section, the surface roughening for SUS304 is larger than that for SUS316 at the same strain level since both MPT and GMO occur in SUS304, but only GMO occurs in SUS316. The FMPT should be taken into account for the calculation of the surface roughening. However, the MPT particularly helps the coarse grain

structure to become more inhomogeneous during plastic deformation. On the other hand, the GMO is also proportional to dislocation density but induces a uniform deformation. Therefore, the effect of MPT should be higher on the roughening mechanism than GMO in stainless steel, especially in SUS 304. When the MPT is spread uniformly, such as for fine grains [20], the surface roughening increase is very low compared to coarse grains with the same strain level. Therefore, MPT could be a factor that enhances the surface roughening behavior, and it is necessary to express surface roughening as a function of F_{MPT} besides F_{GMO}. However, MPT was not considered in conventional models, and these models cannot sufficiently express the surface roughening behavior in thin metal foils of SUS 304. For confirmation, the typical conventional model shown by Equation (1) in the Introduction section was used to fix the experimental results in our previous studies [20,21]. Figure 10 shows the results for room temperature and Figure 11 for elevated temperature experiments. It is seen that there is a discrepancy in the slopes for SUS304 and SUS316 at room temperature, as shown in Figure 10, while the slopes show almost the same tendency in elevated temperatures, as shown in Figure 11. We can thus conclude that the conventional model can accurately fit the experimental results at elevated temperatures but is not accurate for the results of room-temperature experiments since MPT occurs in the latter.
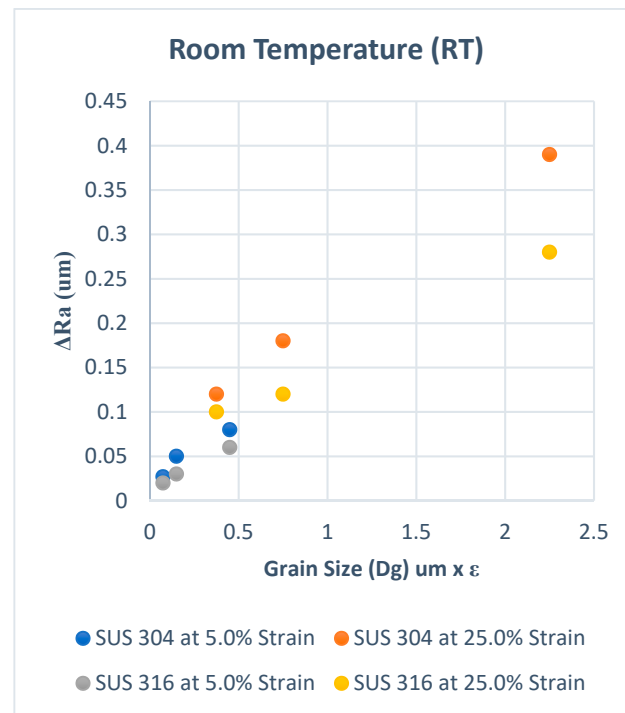

Figure 10. ΔRa versus Dg $\times$ ε at room temperature (RT).

Here, the authors attempt to build a new theoretical model that could express how the MPT and GMO affect the surface roughening behavior in SUS 304 and SUS 316 TMF with various grain sizes. Since the MPT enhances the surface roughness in SUS 304, F_{MPT} was utilized as an additional factor to improve the conventional theoretical model for the prediction of surface roughening. The new theoretical model for the prediction of surface roughening by considering MPT and GMO can be expressed as Equation (2).
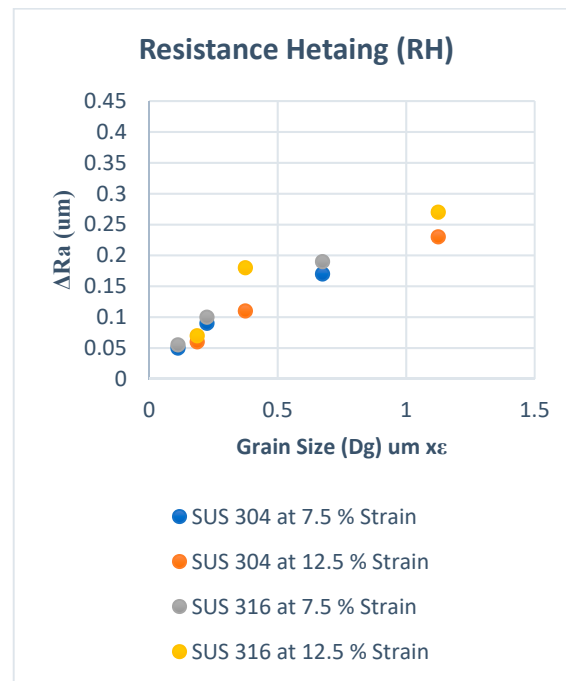
$$\Delta Ra = (F_{MPT} + F_{GMO}) \cdot Dg/t \qquad (2)$$

$$F_{mpt} = C_{mpt} \times (e_p/(Dg)^{1/2}) \qquad (3)$$

$$F_{Gmo} = C_{Gmo} \times (e_p/(Dg)^{1/2}) \qquad (4)$$

where C_{MPT} and C_{GMO} are constants for the volume fraction of MPT and volume fraction of GMO, respectively.

**Figure 11.** ΔRa versus Dg $\times \varepsilon$ at resistance heating (RH).

By substituting Equations (3) and (4) into Equation (2), Equation (5) can be obtained.

$$\Delta Ra = (C_{Mpt} + C_{Gmo}) \times e_p \times Dg^{1/2} \tag{5}$$

The new model is used to fit the experimental results in our previous studies again. The results are shown in Figures 12 and 13. It can be seen that the fitting accuracy was improved for both SUS304 and SUS316 in various grains and conditions of the room and elevated temperatures.
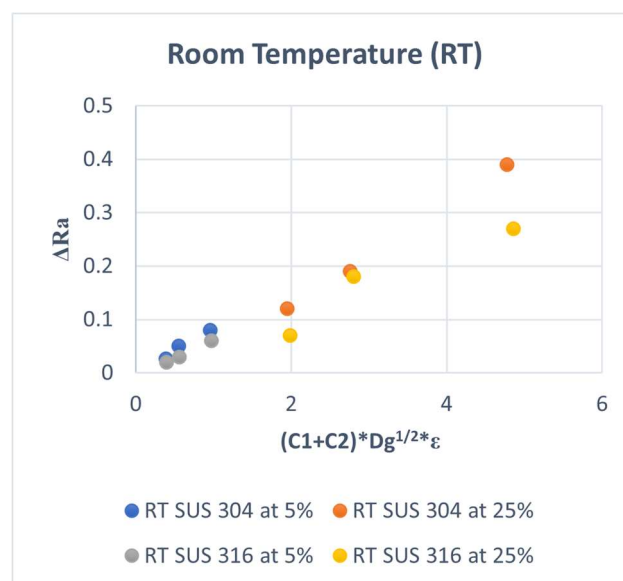
Figure 12. ΔRa versus (C1 + C2) $\times$ g$^{1/2}$ $\times$ E at RT.
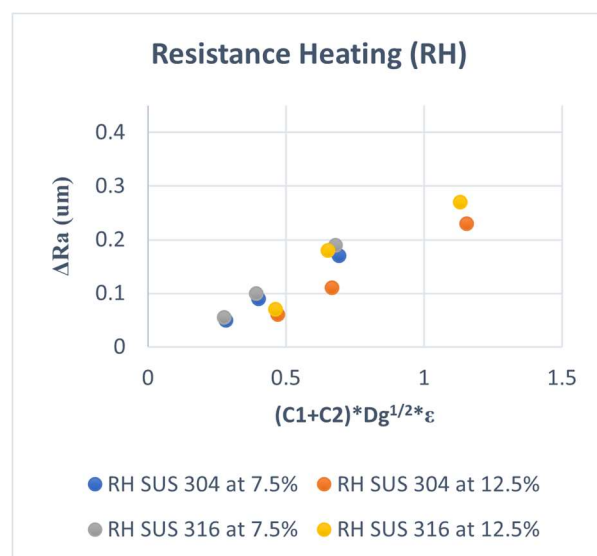
Figure 13. ΔRa versus (C1 + C2) $\times$ g$^{1/2}$ $\times$ E at RH.

The slope for SUS 304 TMF is higher than that of SUS316 at high strain levels at room temperature, but for low strain levels, the slopes are similar, as shown in Figure 12. In the condition of elevated temperature, the slope was similar at a low strain and a high strain level for all kinds of grain sizes, as shown in Figure 13. This means that the model is not yet accurate when a high-volume fraction of the MPT occurs and needs to be improved for this case.

The new model with ΔRa proportional to Dg$^{1/2}$ is better than a conventional model with ΔRa proportional to Dg for the case of SUS 316 TMF without MPT. The different slope in the new model is lower than in the conventional model at room temperature. The slope of the new model of SUS 316 TMF coarse grains at room temperature is 0.056, and the slope of the previous model is 0.125 for coarse grains. The slope of SUS 304 TMF coarse grains in the new model is 0.08, and the slope of SUS 304 TMF coarse grains was 0.177 in the previous model. This means the new model is better than the previous model.

4. Conclusions

1. The volume fraction of MPT and GMO after the tensile test is accounted for, and both FMPT and FGMO are proportional to the plastic strain;
2. The MPT is considered to be a factor that influenced the surface roughening since the SUS 304 TMF showed higher surface roughness than SUS 316 at room temperature, but SUS 304 and SUS 316 TMF were almost the same at elevated temperatures at the same strain level;
3. A new theoretical model that takes FMPT and FGMO into account is proposed, and the difference in the calculated surface roughness for SUS304 and SUS316 at various grain sizes becomes smaller in the new theoretical model than in the conventional models.

References

1. Van Brussel, H.; Peirs, J.; Reynaerts, D.; Delchambre, A.; Reinhart, G.; Roth, N.; Weck, M.; Zussman, E. Assembly of microsystems. *Ann. CIRP* **2000**, *49*, 451–472. [CrossRef]
2. Xue, Z.Y.; Zhou, S.; Wei, X.C. Influence of pre-transformed martensite on work-hardening behavior of SUS 304 metastable austenitic stainless steel. *J. Iron Steel Res. Int.* **2010**, *17*, 51–55. [CrossRef]
3. Gillner, A.; Helrung, D.; Baye, A.; Schepp, F.; Erhardt, R. *Miniarturisierung von Bauteilen Komponenten, 7*; Umformtecniches Kolloquium: Darmstadt, Germany, 2000; pp. 107–116.
4. Milad, M.; Zreiba, N.; Elhalouani, F.; Baradai, C. The effect of Cold Work on Structure and Properties of AISI 304 Stainless Steel. *J. Mater. Process. Technol.* **2008**, *203*, 80–85. [CrossRef]
5. Sundaram, P.A. Deformation -induced surface roughening studies in an AISI 1090 spheroidized steel. *Scr. Metall. Et Mater.* **1995**, *33*, 1093–1099. [CrossRef]
6. Furushima, T.; Aoto, K.; Alexandrov, S. A new compression test for determining free surface roughness evolution in thin metals. *Metals* **2019**, *9*, 451. [CrossRef]
7. Dautzenberg, J.H.; Kals, J.A.G. *Advanced Technology of Plasticity*; Japan Society for Technology of Plasticity/Japan Society of Precision Engineering: Tokyo, Japan, 1984; Volume 1, p. 186.
8. Diani, J.M.; Parks, D.M. Effects of strain state on the kinetics of strain-induced martensite in steels. *J. Mech. Phys. Solids* **1998**, *46*, 1613–1635. [CrossRef]
9. Iwamoto, T.; Tsuta, T. Computational simulation of the dependence of the austenitic grain size on the deformation behavior of TRIP steels. *Int. J. Plast.* **2000**, *16*, 791–804. [CrossRef]
10. Kubo, M.; Nakazawa, Y.; Hama, T.; Takuda, H. Effect of microstructure on surface roughening in stretch forming of steel sheets. *ISIJ Int.* **2017**, *57*, 2185–2193. [CrossRef]
11. Becker, R. Effect of strain localization on surface roughening during sheet forming. *Acta Mater.* **1998**, *46*, 1385–1401. [CrossRef]
12. Huang, J.X.; Ye, X.N.; Xu, Z. Effect of cold rolling on microstructure and mechanical properties of AISI 301LN metastable austenitic stainless steels. *Iron Steel Res. Int.* **2012**, *19*, 59–63. [CrossRef]
13. Choi, J.Y.; Ji, J.H.; Hwang, S.W.; Park, K.T. Strain induced martensitic transformation of Fe-20Cr-5Mn-0,2Ni duplex stainless steel during cold rolling: Effects of nitrogen addition. *Mater. Sci. Eng. A* **2011**, *528*, 6012–6019. [CrossRef]
14. Foecke, T.; Gnaeupel-Herold, T. Robustness of the sheet metal spring back cup test. *Metall. Mater. Trans. A* **2006**, *37*, 3503–3510. [CrossRef]
15. Tsuyoshi, F.; Tetsuro, M.; Manabe, K.-I.; Alexandrov, S. Prediction of Free Surface Roughening by 2D and 3D model considering Material Inhomogeneity. *J. Solid Mech. Mater. Eng.* **2011**, *5*, 978–990.
16. Nie, N.; Su, L.; Deng, G.; Li, H.; Yu, H.; Tieu, A.K. A review on plastic deformation induced surface/interface roughening of sheet metallic materials. *J. Mater. Res. Technol.* **2021**, *15*, 6574–6607. [CrossRef]
17. Yamaguchi, K.; Takakura, N.; Imatani, S. Increase in forming limit of sheet metals by removal of surface roughening with plastic strain (balanced biaxial stretching of aluminium sheets and foils. *J. Mater. Processing Technol.* **1995**, *48*, 27–34. [CrossRef]
18. Mahmudi, R.; Mehdizadeh, M. Surface roughening during uniaxial and equibiaxial stretching of 70-30 brass sheets. *J. Mater. Processing Technol.* **1998**, *80–81*, 707–712. [CrossRef]
19. Kubo, M.; Hama, T.; Tsunemi, Y.; Nakazawa, Y.; Takuda, H. Influence of strain ratio on surface roughening in biaxial stretching of IF steel sheets. *ISIJ Int.* **2018**, *58*, 704–713. [CrossRef]
20. Aziz, A.; Yang, M.; Shimizu, T.; Furushima, T. Effect of Martensitic Transformation and Grain Misorientation on The Surface Roughening of SUS 304 and 316 thin metal foils. *Eng* **2021**, *2*, 372–385. [CrossRef]
21. Aziz, A.; Yang, M.; Shimizu, T.; Furushima, T. The relationship between surface roughening and resistance heating in austenitic thin metal foils of SUS 304 and SUS 316 during tensile test. *Int. J. Res. Eng. Technol.* **2021**, *1*. Available online: https://gnpublication.org/index.php/et/article/view/1942 (accessed on 25 April 2022).
22. Mola, J.; Ren, M. On the hardness of high carbon ferrous martensite. *IOP Conf. Mater. Sci. Eng.* **2018**, *373*, 012004. [CrossRef]
23. Qiu, Z.; Tetsuhide, S.; Tomomi, S.; Ming, Y. Tensile properties and constitutive model of ultra thin pure titanium foils at elevated temperatures in microforming assisted by resistance heating method. *Mater. Des.* **2014**, *63*, 389–397.
24. Tomita, Y.; Shibutani, Y. Estimation of deformation behavior of trip steels-smooth/ringed—Notched specimen under monotonic and cyclic loading. *Int. J. Plast.* **2000**, *16*, 769–789. [CrossRef]
25. Nakagawa, K.; Hayashi, M.; Takano-Satoh, K.; Matsunaga, H.; Mori, H.; Maki, K.; Onuki, Y.; Suzuki, S.; Stao, S. Characterization of dislocation rearrangement in FCC metals during work hardening using X-ray diffraction line—Profile analysis. *Quantum Beam Sci.* **2020**, *4*, 36. [CrossRef]
26. Kishore, K.; Chandan, A.K.; Hung, P.T.; Kumar, S.; Kawasaki, M.; Gubicza, J. On the enhanced hardening ability and plasticity mechanism in a novel Mn-added-CoCrNi medium entropy alloy during high-pressure torsion. *J. Alloys Compd.* **2022**, *9004*, 163941. [CrossRef]
27. Olson, G.B.; Cohen, M. Kinetics of strain—Induced martensitic nucleation. *Metall. Mater. Trans. A* **1975**, *6*, 791. [CrossRef]
28. Tetsu, N. Effect of deformation—Induced martensitic transformation on the plastic behavior of metastable austenitic stainless steel. *Mater. Trans. JIM* **1989**, *30*, 33–45.
29. Moshtagi, M.; Sato, S. Characterization of dislocation evolution in cyclically loaded austenitic and ferritic stainless steel via XRD line profile analysis. *ISIJ Int.* **2019**, *59*, 1591–1598. [CrossRef]

30. Furushima, T.; Tsunezaki, H.; Manabe, K.; Alexandrov, S. Ductile fracture and free surface roughening behavior of pure copper foils for micro/meso -scale forming. *Int. J. Mach. Tool Manuf.* **2014**, *76*, 34–48. [CrossRef]

31. Furushima, T.; Hitomi, T.; Yutaro, H. Fracture and surface roughening behaviors in micro metal forming. In Proceedings of the 17th International Conference on Metal Forming, Metal Forming 2018, Toyohashi, Japan, 16–19 September 2018; Procedia Manufacturing. Volume 15, pp. 1481–1486.

32. Tsuyoshi, F.; Hitomi, T.; Tomoko, N.; Manabe, K.-I.; Alexandrov, S. Prediction of Surface Roughening and Necking Behavior for Metal Foils by Inhomogeneous FE material Modelling. *Key Eng. Mater.* **2013**, *554–557*, 169–173.

33. Tsuyoshi, F.; Tomoko, N.; Kanta, S. A new theoretical model of material inhomogeneity for prediction of surface roughening in micro metal forming. *CIRP Ann.-Manuf. Technol.* **2019**, *68*, 257–260.

34. Kawata, H.; Yasutomi, T.; Shirakami, S.; Nakamura, K.; Sakurada, E. Deformation—Induced Martensite Transformation Behavior during Tensile and Compressive Deformation in Low-alloy TRIP Steel Sheets. *ISIJ Int.* **2021**, *61*, 527–536. [CrossRef]

35. Meng, B.; Fu, M.W.; Fu, C.M.; Chen, K.S. Ductile fracture and deformation behavior in progressive microforming. *Mater. Des.* **2015**, *83*, 14–25. [CrossRef]